

PAPER

## *In vivo* epicardial force and strain characterisation in normal and MLP-knockout murine hearts

To cite this article: M Michaelides *et al* 2015 *Physiol. Meas.* **36** 1573

View the [article online](#) for updates and enhancements.

### Related content

- [Regional assessment of LV wall in infarcted heart using tagged MRI and cardiac modelling](#)  
Zeinab Jahanzad, Yih Miin Liew, Mehmet Bilgen *et al.*
- [Quantification of fibrosis in infarcted swine hearts by ex vivo late gadolinium-enhancement and diffusion-weighted MRI methods](#)  
Mihaela Pop, Nilesh R Ghugre, Venkat Ramanan *et al.*
- [Myocardial elastography under graded ischemia conditions](#)  
Wei-Ning Lee, Jean Provost, Kana Fujikura *et al.*

### Recent citations

- [Molecular and Integrative Physiological Effects of Isoflurane Anesthesia: The Paradigm of Cardiovascular Studies in Rodents using Magnetic Resonance Imaging](#)  
Christakis Constantinides and Kathy Murphy



**IOP** Astronomy ebooks

Part of your publishing universe and your first choice for astronomy, astrophysics, solar physics and planetary science ebooks.

[iopscience.org/books/aas](http://iopscience.org/books/aas)

# *In vivo* epicardial force and strain characterisation in normal and MLP-knockout murine hearts

M Michaelides<sup>1,2</sup>, S Georgiadou<sup>3</sup> and C Constantinides<sup>1,4,5</sup>

<sup>1</sup> Department of Mechanical and Manufacturing Engineering, School of Engineering, University of Cyprus, Nicosia, Cyprus

<sup>2</sup> Lecturer, Department of Sport and Exercise Science, UCLan Cyprus, University Avenue 12-14, Pyla 7080, Cyprus

<sup>3</sup> Department of Agriculture, Histopathological Laboratory, Veterinary Services, Natural Resources and the Environment, Nicosia, Cyprus

<sup>4</sup> Co-Director, Chi Biomedical Ltd., Department of Biomedical Engineering, 36 Parthenonos Street, Apartment 303, Strovolos 2021, Nicosia, Cyprus

E-mail: [Christakis.Constantinides@gmail.com](mailto:Christakis.Constantinides@gmail.com) and <http://lbi-cy.com>

Received 11 January 2015, revised 10 April 2015

Accepted for publication 14 April 2015

Published 9 June 2015



CrossMark

## Abstract

The study's objective is to quantify *in vivo* epicardial force and strain in the normal and transgenic myocardium using microsensors.

Male mice ( $n = 39$ ), including C57BL/6 ( $n = 26$ ), 129/Sv ( $n = 5$ ), wild-type (WT) C57  $\times$  129Sv ( $n = 5$ ), and muscle LIM protein (MLP) knock-out ( $n = 3$ ), were studied under 1.5% isoflurane anaesthesia. Microsurgery allowed the placement of two piezoelectric crystals at longitudinal epicardial loci at the basal, middle, and apical LV regions, and the independent (and/or concurrent) placement of a cantilever force sensor. The findings demonstrate longitudinal contractile and relaxation strains that ranged between 4.8–9.3% in the basal, middle, and apical regions of C57BL/6 mice, and in the mid-ventricular regions of 129/Sv, WT, and MLP mice. Measured forces ranged between 3.1–8.9 mN. The technique's feasibility is also demonstrated in normal mice following afterload, occlusion–reperfusion challenges.

Furthermore, the total mid-ventricular forces developed in MLP mice were significantly reduced compared to the WT controls ( $5.9 \pm 0.4$  versus  $8.9 \pm 0.2$  mN,  $p < 0.0001$ ), possibly owing to the fibrotic and stiffer myocardium. No significant strain differences were noted between WT and MLP mice.

<sup>5</sup> Author to whom any correspondence should be addressed. Co-Director, Chi Biomedical Ltd., Department of Biomedical Engineering, 36 Parthenos Street, Apartment 303, Strovolos 2021, Nicosia, Cyprus.

The possibility of quantifying *in vivo* force and strain from the normal murine heart is demonstrated with a potential usefulness in the characterisation of transgenic and diseased mice, where regional myocardial function may be significantly altered.

Keywords: contractile function, force, strain, piezoelectric crystals, force microsensor.

 Online supplementary data available from [stacks.iop.org/PM/36/071573/mmedia](http://stacks.iop.org/PM/36/071573/mmedia)

(Some figures may appear in colour only in the online journal)

## 1. Introduction

The quantification of the regional forces that neighbouring particles exert on each other (stress) and the material deformation (strain) responses is crucial to cardiac functional characterisation. Correspondingly, regional functional measurements are essential for the study of ischemia, myocardial infarction (MI), and heart failure (HF), where regional mechanics may be significantly altered (De Simone *et al* 1992, Takaoka *et al* 2002).

The relationship between the generated myocardial forces (stresses) and material displacements and deformations (strains) represents the most fundamental description of any material, independent of size or geometry (Demer and Yin 1983). Such mechanical properties are deterministic for the inherent myocardial ability to perform work, and have been demonstrated to be regulators of mechanical growth and remodeling in disease (Omens *et al* 1996).

Invasive and other theoretical methods have been employed over the years to assess and quantify the regional mechanical characteristics of the myocardium. Omens *et al* (1993) and Choi *et al* (2010) evaluated the regional strain distribution using passive inflation. Nevo and Lanir (1994), using theoretical models, demonstrated that the unloaded heart is subjected to residual stresses and strains, and that residual strain has beneficial effects on the left ventricular (LV) diastolic performance while being concurrently responsible for the uniform ventricular stress distribution generated throughout the cardiac cycle. Others (Pelle *et al* 1984, Schmid *et al* 2008, Kroon *et al* 2009) utilised theoretical models to estimate the local stresses and deformations that develop on the LV wall during the heart cycle as well as the elicited haemodynamics.

LV strains have also been previously quantified in contracting hearts of larger animals, such as in canines (McCulloch *et al* 1989, Guccione *et al* 1991), and in rats (Omens *et al* 1996). More recently, advances in magnetic resonance imaging (MRI) techniques, including myocardial spin tagging (Zerhouni *et al* 1988, Axel and Dougherty 1989), displacement encoding with stimulated echoes (DENSE) (Aletras *et al* 1999), and harmonic phase imaging (Osman *et al* 1999), have allowed non-invasive myocardial tracking, motion and strain quantification in humans, and in normal and genetically engineered mice (Rockman *et al* 1991, Franco *et al* 1998, Brede *et al* 2001, Engel *et al* 2004, Wilding *et al* 2005, Epstein 2007, Zhong *et al* 2010).

Despite the numerous publications on *ex vivo* experimental, theoretical, and computational passive myocardial material property characterisation (Pinto and Fung 1973, Demer and Yin 1983, Yin *et al* 1987, Schmid *et al* 1995, Vetter and McCulloch 2000), to our knowledge, only a limited number of prior experimental studies have directly, concurrently, and accurately quantified both the *in vivo* regional strain and force responses of the LV myocardium, due to the underlying difficulties and shortcomings of direct, *in vivo* myocardial force or stress measurements (Huisman *et al* 1980).

Consequently, the purpose of this study was the quantification of the *in vivo* epicardial myocardial force and strain values throughout the cardiac cycle in normal mice, using microsensors and piezoelectric crystals. The temporal evolution of contractile and relaxation force, displacement, and strain are studied at baseline and following afterload challenges.

The developed methodologies are then extended to the study of muscle LIM protein (MLP) knock-out mice (Esposito *et al* 2002) that are associated with an increased LIM role in the cardiac muscle's force response. Correspondingly, the hearts of MLP knock-out mice are used as an animal model of dilated cardiomyopathy (DCM) (Unsold *et al* 2012). The study thus addresses the hypothesis of a decreased evoked force and strain response from the MLP mice compared to wild-type (WT) controls. Therefore, the ability to directly, consistently, and quantitatively compare the evoked force and strain responses in WT controls and transgenic mice emphasises the possible future role of the technique in disseminating observed defects to either the lack of MLP or to the DCM phenotype, and in understanding the etiology of disease progression in terms of the role of the underlying contributors (cardiomyocyte stiffening versus extracellular fibrosis) to the altered global contractile status.

## 2. Materials and methods

### 2.1. Ethics approval

All experimental procedures on mice were designed to avoid unnecessary pain or to minimise any pain or discomfort inflicted on the studied animals. Animal protocols were approved by the Veterinary Services of the Ministry of Agriculture of the Government of Cyprus. All experiments conformed to the European convention for the protection of vertebrate animals used for experimental and other scientific purposes (Council of Europe Number 123, Strasbourg 1985).

### 2.2. Overview of mouse studies

The developed methodologies were applied to a cross-strain (C57BL/6) knock-out mouse model of MLP. To quantify the control force/strain values at the various genetic backgrounds, twenty six male C57BL/6 (mean age = 11 weeks, mean weight = 24.4 g), five male 129/Sv mice (mean age = 13.8 weeks, mean weight = 25.0 g), five male WT control C57 × 129Sv (mean age = 24.5 weeks, mean weight = 29.6 g), and three male MLP knock-out mice (mean age = 10.3 weeks, mean weight = 25.9 g) were studied in total. All mice were kept in polypropylene cages (2–3 mice per cage) with food and water provided *ad libitum*. The mice were maintained on a 12–12 h dark–light cycle.

### 2.3. Mouse physiology and animal preparation

The mice were induced for 2–3 min using 3–5% isoflurane (ISO) (Nicholas Piramal (I) Limited, London, UK). Anaesthesia was maintained by inhalation of 1.5% ISO (v/v) delivered via a nose cone (having a volume of 1  $\mu$ l and a 0.2  $\mu$ l of dead space). For the studied mice, either a 100% O<sub>2</sub>, or a 50:50 O<sub>2</sub>/N<sub>2</sub>O mixture was administered with ISO (Constantinides *et al* 2011a). Breathing and ECG were recorded using a Biopac recording system (Biopac Systems Inc, USA), as reported earlier (Constantinides *et al* 2011a). The heart rate was maintained at between 450–550 bpm approximately for all conducted experiments. The temperature was maintained at adequate levels (at approximately 37°C) using a rectal temperature sensor (Physitemp, NJ, USA) connected to a temperature controller (Digi-Sense, Cole Parmer Inc., IL, USA).

#### 2.4. Mouse tracheotomy and open chest microsurgery

The animals were intubated using a procedure that was described previously (Constantinides *et al* 2011a). Through a midline sternotomy, and with the aid of a rib retractor (Roboz Surgical Instruments, Gaithersburg, MD, USA), the chest was maintained opened, exposing the heart. The ventilator respiration rate was set at 135–138 bpm, before and after intubation.

To validate the methodology of force recordings, simple interventions (transient afterload increases via partial aortic occlusions) were performed in two C57BL/6 mice with consistent response patterns, over multiple efforts. In such cases, the aorta was exposed and a silk thread loop allowed its tethering, and partial occlusion and reperfusion, during concurrent force recordings.

#### 2.5. Piezoelectric crystal placement

Exposure of the myocardium allowed placement of the MRI compatible piezoelectric crystals (Sonometrics, London, Ontario, Canada). Three types of available crystals were used: commercially available crystals with epoxy coating (diameters of 0.5–0.7 mm (42-AWG-Cu type)) were initially used, followed by the use of crystals with thin sealant coverage, and crystals without any epoxy coating (bare) (diameter of approximately 0.2 mm). The latter two types were specially made by Sonometrics to assist our experimental effort with rodent measurements. All of the types of crystals used were sutured on the epicardial surface. For all experiments only two sensors were placed in either the basal (about 1 mm below the large vessels), middle (about 2 mm over the apex, and 1–2 mm below the base of the heart), or apical areas of the LV wall (figure 1). To ensure adequate communication, crystals were sutured facing each other (with a minimum distance of 1 mm apart) and were covered with gel (Signa Gel, Parker Laboratories, Fairfield, NJ, USA). They were subsequently connected to an analogue sonomicrometer unit (Sonometrics, London, Ontario, Canada). Recordings were acquired at a 1 kHz sampling rate via an eight channel ADI acquisition system (ADI Instruments Inc., USA), and were displayed and saved with the use of PVAN (ADI Instruments, USA). Consistency in crystal placement was based on microsurgical expertise, and on anatomical landmarks of the murine epicardial morphology.

#### 2.6. Force sensor placement

The AE-800 force sensor (AE801, Kronex, CA, USA) was attached (with the cantilever element in a horizontal position, in a direction parallel to the long axis of the exposed heart) to a specialised adjustable platform. A silk thread (Ethicon USP 8.0, NJ, USA) was sutured on the different areas of the antero-lateral epicardial LV wall (basal, middle, apical). The end of the silk thread was folded to create a loop (through a puncture of the epicardium). A thin metallic wire (length = 9.88 cm, diameter = 0.13–0.25 mm) with hook ends was attached to both the silk-threaded epicardial loop and to the force sensor cantilever (figure 1). The force sensor was subsequently connected to the half-bridge circuit of the microstrain recording device that consisted of two active resistors. When the tip of the beam was deflected, the total force sensor resistance changed in accordance with the exerted mechanical force. The attachment of the cantilever on the myocardium (using a silk thread at superficial depths, visible to the human eye from the epicardial surface) did not result in force drifts or non-constant force recordings over time.

The proper level placement of the cantilever platform (before the onset of recordings) ensured that the lowest force state of the epicardium matched the end-diastolic state.

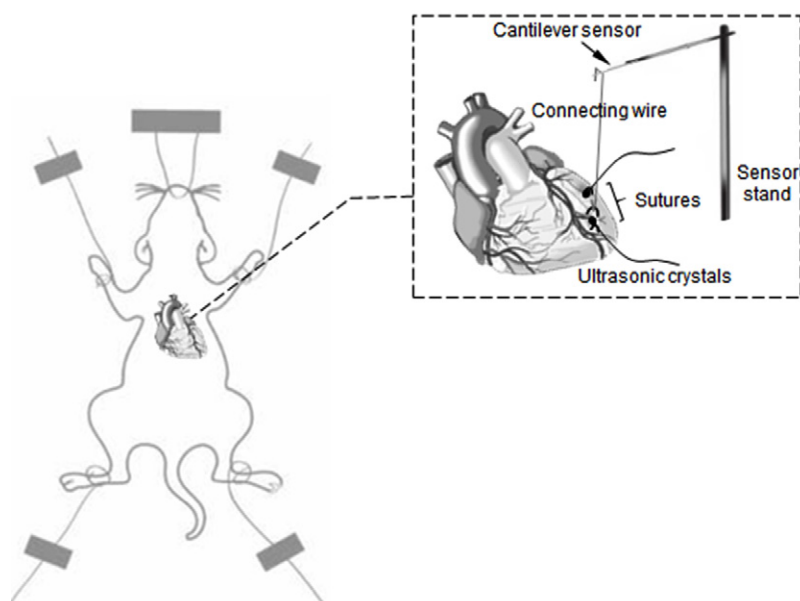


**Figure 1.** Microsurgical implementation of ultrasonic crystal and force sensor placements. Schematic representation of the anaesthetised mouse and the piezoelectric crystal implantation scheme. Up to four sensors can be placed concurrently but recordings are only allowed from two—to minimise the effects of anaesthesia, surgery, and trauma, only two (one-pair) crystals were added on the myocardium at each experimental setting. The schematic also depicts the force sensor attachment at the epicardial regions of the exposed LV epicardium (with the force sensor assembly showing the force sensor and positioning platform, the silk thread sutured on the epicardium, and the silver-connecting wire). Every effort was taken during recordings for accurate positioning of the sensor, thereby avoiding lifting of the heart.

Appropriate cantilever placement was also confirmed in a number of studied animals at the end of the recording period, immediately after euthanasia (post-mortem state), where the cantilever force returned to its flat zero-baseline value.

### 2.7. Displacement and force recordings

Recordings were conducted over 10 min intervals using the ADI recording system (piezoelectric crystals) via connection to a microstrain recording device (Vishay, Raleigh, NC, USA) (force sensor). Three cohorts of mouse data were collected: separate piezoelectric displacement, separate force, and concurrent force-displacement recordings. For the assessment of the temporal constancy of the force and strain values (over the 10 min intervals), separate (but serially recorded in time) force and displacement datasets were collected and analysed.

### 2.8. Strain and force calculations

Both the piezoelectric crystals and the force sensors were calibrated prior to each experimental procedure, yielding voltage versus displacement (or force) calibration curves. No quantisation effects (or errors associated with such phenomena) could result from the use of the specific sonocrystals employed. For the piezoelectric crystals, the sonomicrometer's

built-in calibration settings were used. Displacement was converted to percentage strain (in accordance to a resting diastolic displacement, as explained in the data analysis section below). For the force sensor, dedicated weights comprised of lead pellets (ranging in weight from 0.1–2.4 g) were used (with similarly placed threaded-loop sutures, as those used *in vivo*, in an effort to emulate the *in vivo* setup) to generate force versus voltage calibration curves.

### 2.9. Data analysis

All datasets were exported in text files and were subsequently analysed using MATLAB (Natick, MA, USA) with routines written in-house. Specifically, peak detection algorithms allowed maxima and minima recordings, and estimations of contraction, relaxation force, and displacements over 1 s time intervals. Given the large inter-crystal distance (1–2 mm) compared to the size of the heart (whereby the curvature of the myocardium was ignored), strain (or interchangeably and equivalently, fractional shortening) ( $\epsilon$ ) values were estimated according to:

$$\epsilon = \frac{\Delta l}{l_0} \quad (1)$$

where  $\Delta l$  represents the maximum or minimum crystal distances during relaxation or contraction, respectively, and  $l_0$  the initial (resting) crystal separation, determined as the end-diastolic displacement within each analysed cycle.

### 2.10. Motion variability analyses

With the proposed setup for force recordings, the inherent cardiac motion during each cycle causes a temporally varying orientation of the connecting wire (and thence, changes in the direction of the total force recorded). Furthermore, rigid body movements of the mouse or the mouse heart thereof (primarily owing to breathing or gasping chest motion) may affect such force measurements. Rigid body motion effects were reduced to a minimum during force recordings through: (a) stabilisation of the mouse post-microsurgery, before the onset of recordings, (b) proper anaesthesia maintenance, (c) calculation of contractile (end-systolic (ES) and end-diastolic (ED)) or relaxation (ED–ES) force differences.

The effects on the recorded (or calculated) total mean force during the cardiac cycle, and owing to the beat-to-beat variability of motion (as such may affect the average force estimation, over 1 s or 10 s intervals), were quantified, and the total mean force was decomposed into the heart's material (fibre) coordinate system, using independent movie recordings, photography, and tracking, as described in the supplementary data ([stacks.iop.org/PM/36/071573/mmedia](http://stacks.iop.org/PM/36/071573/mmedia)).

### 2.11. Histopathologic evaluation

*Control mice:* for the histopathologic evaluation of myocardium and assessment of ischemic or necrotic damage, hearts (one control C57BL/6, and two C57BL/6 hearts from experiments with piezoelectric and force sensors) were harvested and placed into a fixative solution (10% formalin) for 5–11 d. Contiguous sections from all of the samples were cut every 5  $\mu\text{m}$ . More than 25 slides of each sample were stained with hematoxylin and eosin, focusing primarily on the epicardial and transmural areas where the suture threads were placed.

*Wild-type and MLP mice:* all of the WT and MLP-knockout hearts were harvested at the end of the experimental procedures, post-euthanasia, and were placed into a fixative solution

(10% formalin) and stored. Two WT and two MLP-knockout hearts were embedded and processed. Contiguous slices were then sectioned from all samples with a microtome, every  $5\ \mu\text{m}$ , along the heart's short axis. More than 60 slides of each sample heart were stained (covering the basal, middle, and apical areas of the fixed, processed hearts) with picro sirius red staining, in an effort to assess increased extracellular matrix deposition in MLP-knockout hearts, compared to the WT controls.

### 2.12. Statistical analyses

All results are reported as mean  $\pm$  standard deviation (SD). The constancy of systolic and diastolic forces and strain values is reported as within (the period of recording for each mouse), and between (averaged estimates for all the mice studied during the effective period of recording) the coefficient of variabilities (e.g.  $CV_{HR} = 100 \times SD_{HR}/Mean_{HR}$ ) of the averaged 10 s estimates, over 10 min intervals of recording. The assessment for the existence of significant variability for all such recorded parameters was achieved using two-way analysis of the variance (ANOVA) tests (XLSTAT, Addinsoft, USA) (genetic lineage compared for force and mechanical strain at middle myocardium, and mechanical strain compared at three myocardial levels in control (C57BL/6) mice), and with Tukey's post hoc analysis tests for multiple determinations.

## 3. Results

Figure 1 depicts in a diagrammatical and pictorial form, the placement of piezoelectric crystals on the LV epicardium and the force sensor assembly. In the mouse piezoelectric studies, two or four crystals can be placed (but only two can become active at any instant in time) in any preferred arrangement (longitudinal, circumferential), however, the reported results refer to longitudinally placed pairs of crystals. Additional cohorts of mice allowed separate or concurrent (to displacement) recordings of epicardial force, using the micro-cantilever force sensor setup of figure 1. Both the crystals and force sensors were sutured on the epicardium. Hematoxylin and eosin histological staining post-mortem revealed no evidence of ischemic presence, eliminating the possibility of myocyte necrosis (or other local dysfunction) owing to the surgical procedures or trauma (during the studied period), as shown in figure 2.

Figure 2 also confirms myocardial fibrosis (using histological picro sirius red staining along short axis orientations) exemplified by the increased deposition of the extracellular matrix (collagen, connective tissue) in MLP knock-out mice, in comparison to the WT C57  $\times$  129Sv controls, or to normal C57BL/6 control mice. The histological examination of the left and right ventricular myocardial muscle of MLP-mice revealed muscle thinning and enlargement of the ventricular cavities, in support of the dilated cardiomyopathic phenotype.

Figure 3 shows corresponding schematic representations of the heart as well as the principle myocardial force directions (cardiac fiber axes) (including radial, circumferential, and longitudinal) and associated developed forces. Shown also in this figure are typical force and displacement recordings over a 1 s time interval from an *in vivo*, normal C57BL/6 mouse. Simple afterload interventions (partial aortic constriction) performed in normal C57BL/6 mice indicated initial force reductions (immediately after constriction) owing to the progressive LV and right ventricular (RV) chamber emptying, followed by a sudden dilation of the ventricular chambers (soon after aortic reperfusion), owing to rapid chamber filling. Numerous subsequent forceful contractions followed, before baseline functional activity was restored (figure 3).

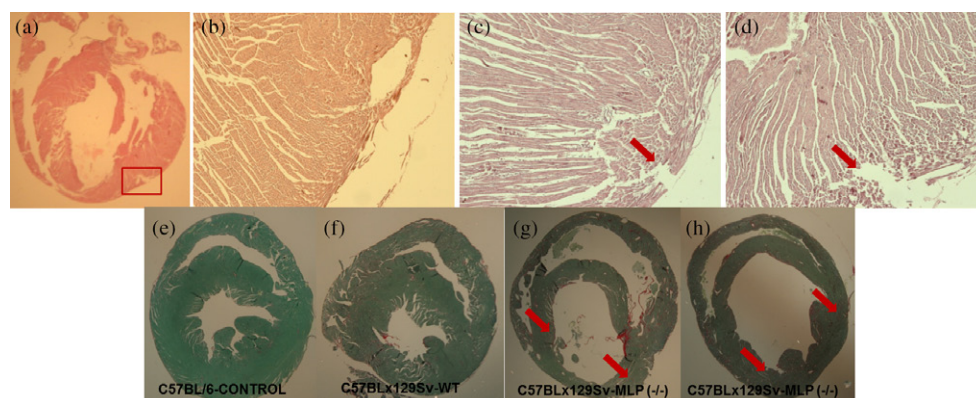


**Figure 2.** Histological tissue evaluation. (Top) Hematoxylin and eosin histology revealed no evidence of ischemic presence, eliminating the possibility of myocyte necrosis due to the surgical procedures; (bottom) picro sirius red, mid-ventricular short axis histology stained slices, revealing myocardial thinning and increased deposition of extracellular matrix in MLP-knockout mice. (a) Typical (post-mortem) long axis view of the myocardium that underwent surgical intervention for sensor placement. The region of interest (box) denotes the area from which stained slices are visualised; (b) stained slice showing an intact control epicardial region. (c, d) stained histology slides showing the sites (arrow) of the inserted epicardial sutures for the force sensor placement. No indication of ischemia is observed in the area. Picro sirius red stained slices of (e) a control C57BL/6 heart, (f) a wild-type C57  $\times$  129Sv heart, and (g, h) two dilated cardiomyopathic hearts from C57  $\times$  129Sv MLP knockout mice with increased fibrosis (arrows).

The force measurement methodology was applied to normal C57BL/6 ( $n = 16$ ), 129/Sv ( $n = 9$ ), WT control (C57  $\times$  129Sv) ( $n = 5$ ), and MLP-knockout mice ( $n = 3$ ). Temporal variations of the recorded force, and strain (over 10 min intervals), for normal C57BL/6, WT, and MLP-knockouts are depicted in figure 4. Strain values are referred to the estimated ED, resting crystal separation. Average recordings over 10 s periods are plotted as these determine the force and strain evolutions of the epicardium during systole (contraction) and diastole (relaxation).

A quantitative assessment of the effects of motional variability (in two normal C57BL/6 and 129/Sv mice (data not shown)) during beat-to-beat, 1 s and 10 s time-intervals, is shown in figure 5 (for the basal, middle, and apical left ventricular areas of a normal C57BL/6 mouse).

Minimal effects were computed for changes in the direction of the wire (as connected to the cantilever and myocardium) as a result of such beat-to-beat variability (maximum excursions of the detected hook positions were less than 0.5 mm for C57BL/6 and 129/Sv studied mice, leading to angular deviations of less than  $0.29^\circ$ ). Such global motion effects were thus ignored.

The effect of force averaging (for data analysis and reporting purposes) over 1 s and 10 s intervals was also quantified in plots showing deviations of the median, 25%, and 75% quantile values from the estimated mean, and maximum and minimum data values (over the studied intervals). Such deviations ranged between 0.65 and  $-0.94$  mm (for the two studied C57BL/6 mice) and between 0.30 and  $-0.35$  mm (for the two studied 129/Sv mice), indicative of minimal compound errors associated with statistical mean force reporting, in comparison to actual beat-to-beat force estimates (figure 5).

Table 1 summarises mouse strains, sample sizes, and relevant statistical tests conducted. The findings demonstrated constancy of the maximum evoked mean contractile epicardial

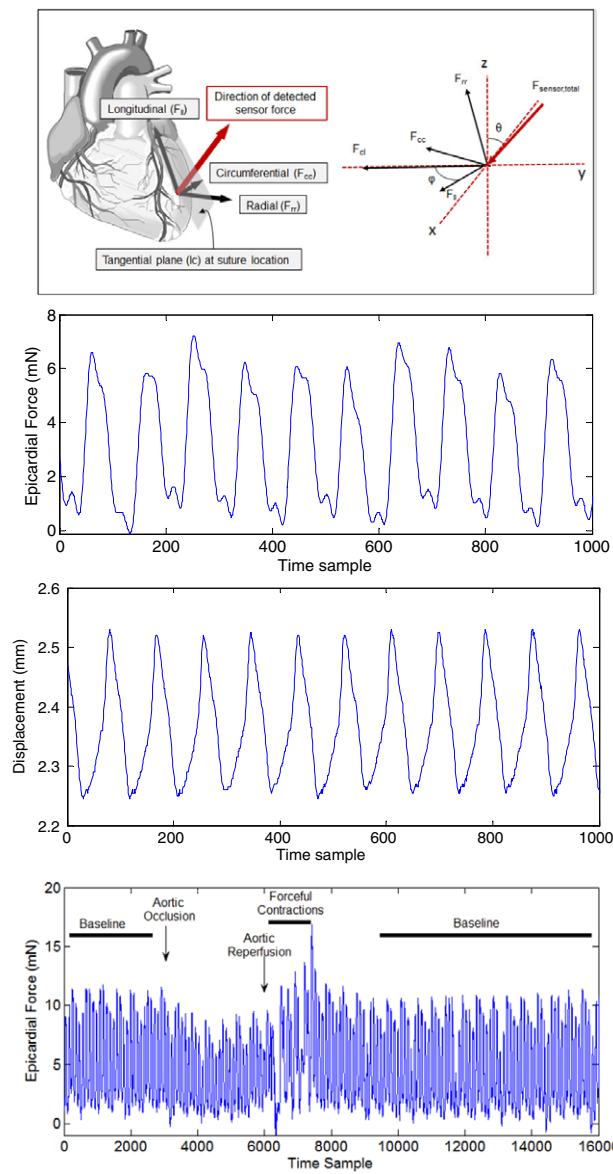


**Figure 3.** *In vivo* recordings of total epicardial ventricular force and displacements. (Top row) Schematic representations of the heart depicting the anterior epicardial force measurement locations, the principle myocardial force directions (radial, circumferential, longitudinal), and the direction of the detected cantilever force. The angle  $\theta$  represents the azimuthal angle between the connecting wire and the plane tangential to the surface of the heart (at the suture locus); the equatorial was maintained at  $90^\circ$ ;  $\varphi$  represents the angular deviation of the circumferential component along the longitudinal-circumferential axis. (Second and third rows) Typical *in vivo* force and displacement recordings (from different mice), over a 1 s period from (different) C57BL/6 mice; (fourth row) epicardial force recording from a control C57BL/6 mouse from an anterior middle-epicardial location during baseline, and after partial aortic occlusion and reperfusion.

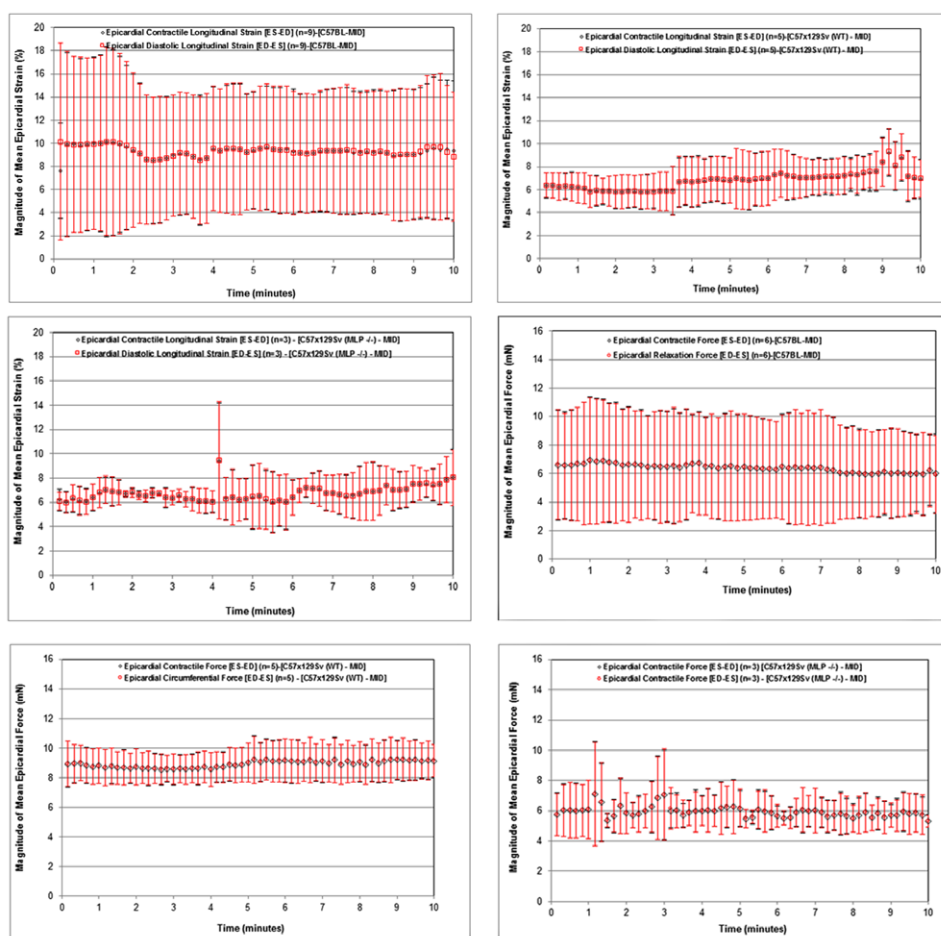


**Figure 4.** Strain and force temporal variation patterns. The temporal variation of *in vivo* contractile and relaxation strain and force values. The magnitude of mean contractile (end-systolic to end-diastolic) and relaxation (end-diastole to end-systole) strain and force variations from the implanted piezoelectric crystals and force sensors on the (first column) middle C57BL/6, (second column) middle wild-type C57 × 129Sv, and (third column) middle MLP-knockout C57 × 129Sv murine myocardium, over 10 min of recordings. Reported results reflect averages and SD values over 10 s time intervals.

longitudinal strains (over the 10 min intervals) of  $6.57 \pm 0.7/9.29 \pm 0.43/5.03 \pm 0.72\%$  (for C57BL/6 mice in the basal, middle, and apical areas, respectively),  $4.82 \pm 0.65\%$  (for 129/Sv mice in the middle LV areas),  $6.78 \pm 0.74\%$  (for WT C57 × 129Sv controls in the middle LV areas), and  $6.74 \pm 0.6$  (for MLP knock-out mice in the middle LV areas).

The force sensor results (figure 6) yielded mean epicardial forces (over the 10 min intervals) with values of  $3.07 \pm 0.17$ ,  $6.39 \pm 0.26$ , and  $5.47 \pm 0.24$  mN (in the basal, middle, and apical areas of C57BL/6 mice),  $7.79 \pm 0.38$  mN (in the middle LV areas of 129/Sv mice),  $8.92 \pm 0.22$  mN (in the middle LV areas of WT controls), and  $5.91 \pm 0.35$  mN (in MLP mice). Figure 6 also depicts the decomposed total myocardial force along the radial, circumferential, and longitudinal directions, for all of the mouse strains studied.

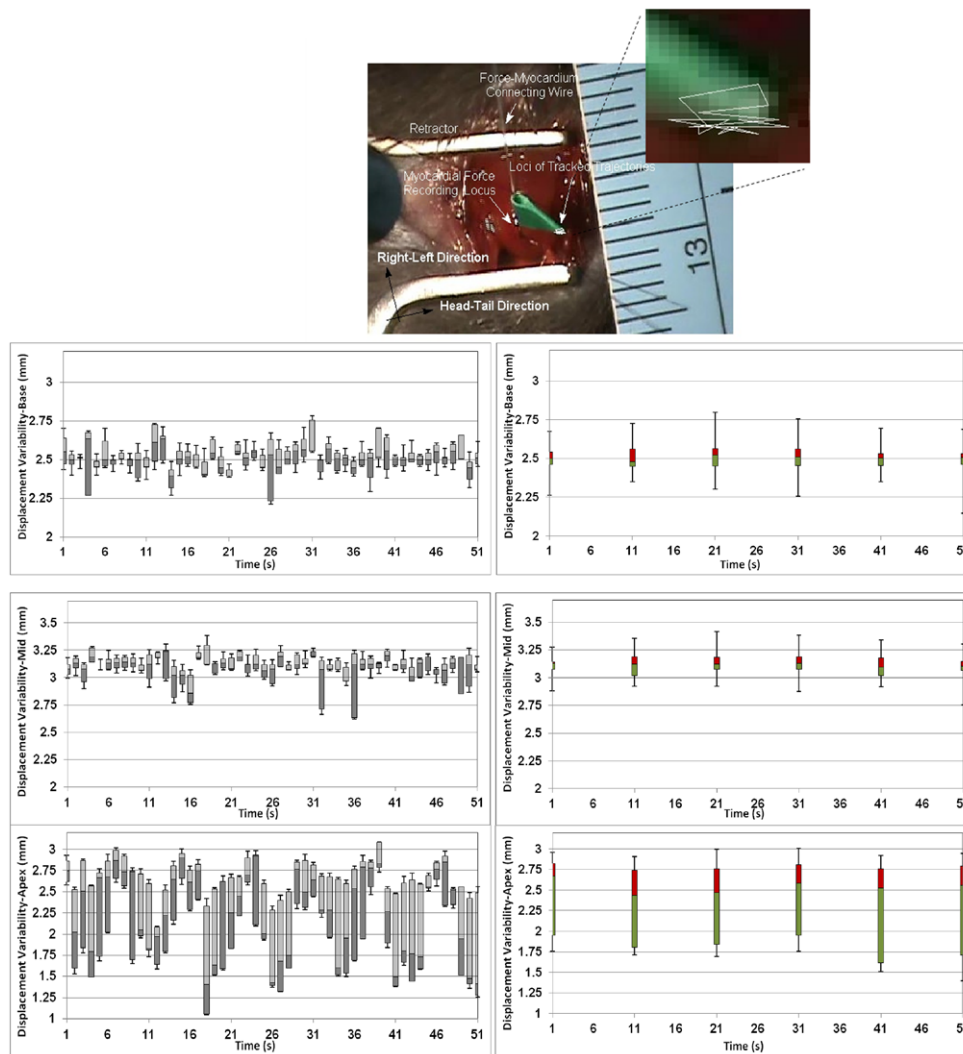


**Figure 5.** The assessment of the relative contribution of global motion effects to total recorded force. Variational analysis of the *in vivo* epicardial motion in a typical C57BL/6 mouse. (Top row) Photographic representation of the force sensor wire attachment on the anterior epicardium. The green flag and the wire hook attachment were spatially tracked over multiple cardiac cycles (a typical set of trajectory patterns is shown in the upper right corner) in the basal, middle, and apical regions of the studied C57BL/6 and 129/Sv murine myocardium; (second row to bottom) presented are (left) basal-middle-apical beat-to-beat displacement variability plots, and (right) corresponding plots of mean displacement estimates over 10s intervals. Bar-graphs represent 1st quantile-median (dark gray or green), and 3rd quantile-median (light gray or red), with error bars representing the minimum and maximum values in each period.

Within and between the CV ranges/mean values for contractile forces were 6.7–15.8% and 5.5% (base—C57BL/6), 3.2–18.3%, and 4.1% (middle—C57BL/6), 6.8–15.7% and 4.5% (apex—C57BL/6); 2.6–21.8% and 4.8 % (middle—129/Sv), 2.3–6.4% and 2.5% (middle—C57 × 129Sv), and 2.2–13.8% and 5.9% (middle—MLP).

**Table 1.** Summary of the completed statistical tests listing demographic details of mouse strains, myocardial locations, and sample sizes.

CV analyses ANOVA	C57BL/6	129/Sv	C57 × 129Sv (WT)	MLP
Displacement/Strain	Basal ( <i>n</i> = 5)	—	—	—
	Middle ( <i>n</i> = 9)	Middle ( <i>n</i> = 4) <sup>a</sup>	Middle ( <i>n</i> = 5)	Middle ( <i>n</i> = 3)
	Apical ( <i>n</i> = 5)	—	—	—
Force	Basal ( <i>n</i> = 5)	—	—	—
	Middle ( <i>n</i> = 6)	Middle ( <i>n</i> = 5)	Middle ( <i>n</i> = 5)	Middle ( <i>n</i> = 3)
	Apical ( <i>n</i> = 5)	—	—	—

<sup>a</sup> Four mice were studied in total—owing to technical difficulties with the displacement during part of the recording period, the elicited temporally varying average strains reflect the mean from 2–4 mice datasets.

Corresponding within and between the CV values for contractile strains ranges/mean values were 8.9–20.6% and 10.7% (base—C57BL/6), 2.8–29.0% and 4.7% (middle—C57BL/6), 7.8–41.0% and 14.3% (apex—C57BL/6); 6.3–21.6% and 11.1% (middle—129/Sv), 6.3–21.8% and 11.0% (middle—C57 × 129Sv), and 6.5–28.5% and 8.9% (middle—MLP).

The statistical variability for contractual (ES–ED) and relaxation (ED–ES) forces and strains was assessed using the analysis of variance tests (ANOVA) followed by Tukey's honest significance difference (HSD) tests for multiple determinations. The ANOVA variance tests demonstrated significant variability differences in the recorded forces and strains during both the contraction and relaxation phases of the cardiac cycle ( $p < 0.0001$ ), at different locations of the LV myocardium (both in C57BL mice and in mid-myocardial locations of normal 129/Sv mice). Furthermore, significant variability differences were also noted in the recorded forces and strains in the middle-myocardial regions of C57BL, WT C57 × 129Sv, and MLP mice.

#### 4. Discussion

The laminar composition of the myocardial architecture and its tortuous myofibre composition (Takayama *et al* 2002) add tremendous complexity in its structure and mechanical function. While prior attempts were successful in invasively measuring displacement using piezoelectric crystals (Villarreal *et al* 1988, Lima *et al* 1993, Yeon *et al* 2011) and other methodologies (Waldman *et al* 1985, McCulloch *et al* 1989), attempts to measure myocardial force or stress languished, and the feasibility for successfully performing such measurements remained elusive.

Mechanical strain and stress, as the basic determinants of systolic and diastolic function, are also regarded as long-term prognostic biomarkers. The ability to conduct concurrent material strain and force measurements in real time is certainly advantageous for the direct mechanical characterisation of the tissue providing new opportunities for direct, constitutive law quantification in comparison to non-invasive techniques, such as MRI and echocardiography. On the other hand, the inherent measurement resolution of this invasive, epicardial technique is limited by the physical size of the recording sensors. Correspondingly, and the measurements are susceptible to motion-induced misalignment effects as compared to the superior spatial resolution of recordings in MRI and ultrasound, in relation to the deformation tensor formulation and transmural strain estimation.

Piezoelectric crystals, tagging, and DENSE-MRI, have been extensively used to quantify myocardial displacement and strain. Gilson *et al* (2005) reported values of –0.5 mm (basal), –0.25 mm (middle), and 0.06 mm (apical), in mice, in agreement with our corresponding

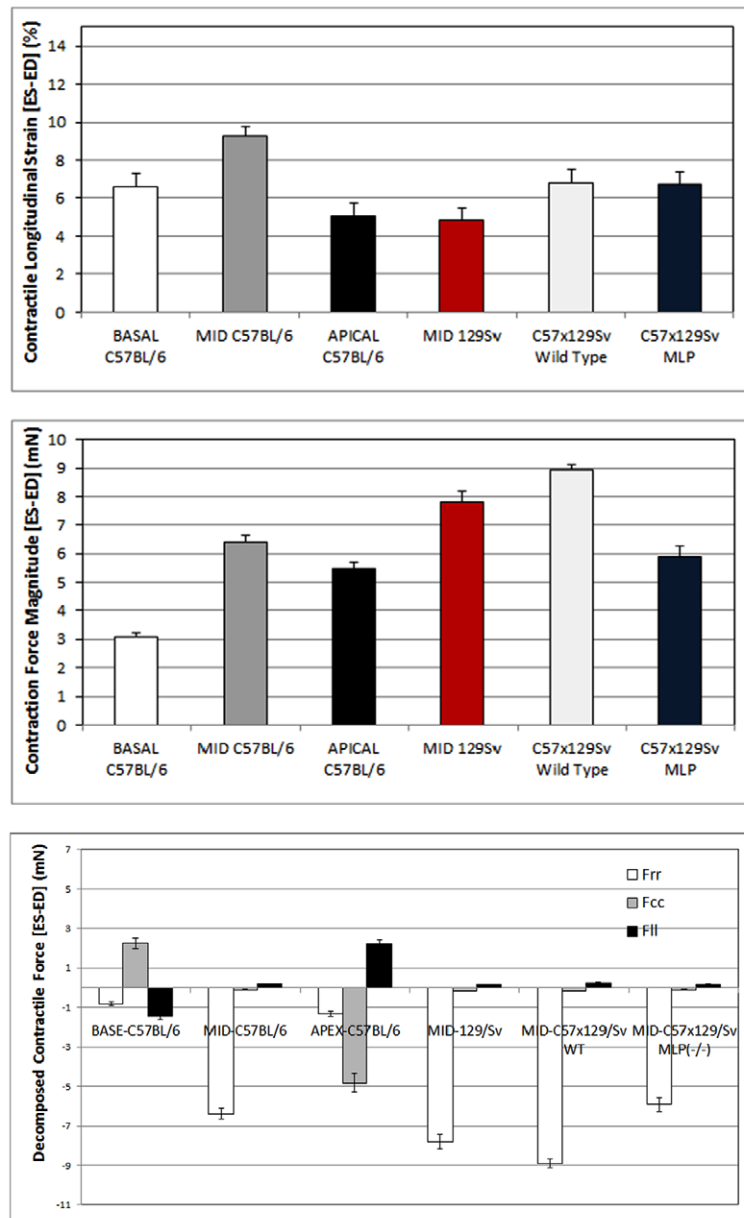


**Figure 6.** Strain and force comparisons in normal and transgenic mice. Strain and force (total, decomposed) comparisons in normal, wild-type (WT) and MLP transgenic mice. (Top, middle) Mean contractile longitudinal strain and mean magnitude of total recorded (contractile) force over basal, middle, and apical myocardial areas in normal C57BL/6, 129Sv, WT C57 × 129Sv and MLP-transgenic mice; (bottom) decomposed force representation along radial ( $F_{rr}$ ), circumferential ( $F_{cc}$ ), and longitudinal ( $F_{ll}$ ) myocardial directions.

estimated mean and absolute displacement values ranging from 0.1–0.15 mm, 0.1–0.23 mm, and 0.07–0.11 mm, using piezoelectric crystals. The peak contractile longitudinal strain in mice has also been recently reported to be  $18 \pm 14\%$  using DENSE-MRI (Zhong *et al* 2011)

that is higher than our reported values of  $4.8 \pm 0.6$ – $9.3 \pm 0.4\%$ . The underestimation can be justified by the fact that only longitudinal strain values ( $\epsilon_{ll}$ ) are reported in this study and that there may be possible differences in the scale of the spatial measurement, compared to the total (composite) strain ( $\epsilon_{\text{tot}} = \sqrt{\epsilon_{ll}^2 + \epsilon_{cc}^2 + \epsilon_{rr}^2}$ ) reported in MRI publications. Despite the differences in reported values, the spatial pattern of developed strain agrees closely to that reported based on MRI (Zhong *et al* 2011).

Additionally, recent advances in fabrication technology have allowed the construction and commercialisation of compact, miniature cantilever force microsensors for force measurements of the order of nN. The use of such sensors has been mainly limited to *in vitro* studies where prior attempts evaluated the force production of skinned fibres from skeletal, smooth muscle (Alessi *et al* 1992, Wu *et al* 1998, He *et al* 2000, Yamaguchi and Takemori 2001), and *in vitro* cardiac muscle studies (Hanley and Loiselle 1998, Baker *et al* 2001).

The technique's underlying advantages include the facts that measurements are directly obtained from the epicardium as these pertain to the force-generating ability of cardiomyocytes. To this extent, measurements are more relevant to cellular force generation and its modulation owing to the tethering of the cytoskeleton to the extracellular matrix, compared to globally averaged estimates of pressures and volumes recorded using invasive catheters placed within the ventricular chamber.

The total force measurements ( $F_{\text{tot}}$ ) from this study ranged between 3.1–8.9 mN, and are, to our knowledge, some of the first ever recorded from the active, *in vivo* epicardium. Any force measurement reported using the presented methodology would be a very complicated reflection of LV force development, comprising an active fibre, a passive fibre, and a passive inflow filling component, in accordance with:

$$F_{\text{tot}}(t) = F_{\text{active, fiber}}(t) + F_{\text{passive, fiber}}(t) + F_{\text{passive, inflow-filling}}(t)$$

These epicardial force measurements are reflective of the developed force at a spatial position located between the loci of the placed piezoelectric crystals (spanning 0.5–1 mm). The technique's feasibility to detect responses in challenged animals was also demonstrated with transient afterload increases, post-aortic occlusion, as direct manifestations of the Frank–Starling law. Reported force estimates were based on the subtraction of peak systolic and diastolic cantilever displacements and they have not accounted for possible diastolic or peak systolic pressure variations under loading condition variations during the conducted experimental studies. Based on two prior elaborate studies on the effects of anaesthesia on mean arterial blood pressure (Constantinides *et al* 2011a) and haemodynamics (Constantinides *et al* 2011b), the authors have established optimal protocols of invasive studies under anaesthesia in normal C57BL/6 mice, ensuring the constancy of such parameters over extensive periods post-induction. Furthermore, significant differences in strain ( $\epsilon_{ll}$ ) and force measurements were observed in different areas of normal mice of the same or different genetic strain, directly attributed to intra- or interspecies fibre architectural differences. In addition, motional variability analyses indicated that the effects on total force from the beat-to-beat cardiac variability were minimal. More prominent beat-to-beat variability effects were consistently observed in apical (compared to basal or middle myocardial) areas.

Based on the presented results, it is shown that little circumferential or longitudinal force is noted in the middle areas of the myocardium. Instead, the prominent force component is along the radial direction. Similarly, primarily apical (and to a lesser extent basal) areas are associated with developed circumferential (torsional) and compressive (longitudinal) force components (of opposite direction) during the systolic phase of the cycle.

Functional results also exhibit significant reductions in elicited *in vivo* forces in MLP-/- mice (age >6 months) compared to WT controls (age >2.5 months), possibly owing to a stiffer, fibrotic myocardium, as reported earlier in skinned papillary muscles of 12 week MLP-mice (Unsold *et al* 2012). These results are also in agreement with the histological phenotype of MLP mice, exhibiting prominent cyto-architectural disorganization and disruption with increased collagen deposition and fibrosis (Arber *et al* 1997, Knoll *et al* 2010, Unsold *et al* 2012). The presented results also indicate increased total force values from the middle myocardium of WT-control mice, in comparison to middle-myocardial forces from normal C57BL/6 and 129/Sv mice. The findings were likely attributed to secondary strain (breed) differences or to the age of such mice, compared to the age of the normal animals studied (approximately 3–3.5 months). Additionally, contrary to reported results on radial strain, exhibiting significant reductions in MLP-mice compared to controls (Esposito *et al* 2000), our reported results show insignificant longitudinal strain differences in WT and MLP mice.

One of the study's primary limitations is the important unbalance between the mouse strains and the number of mice studied. This certainly guarantees additional investigations with increased and balanced sample sizes in regard to the strain type and myocardial locations evaluated. Correspondingly, the non-significant results elicited from some group comparisons may be also attributed to type II errors. Additionally, the sample size for some cohort studies (particularly for the MLP-mice) is rather low, and inferences drawn from such data must be interpreted with caution. An additional study limitation includes the possible inconsistencies of force measurements. The complex cardiac geometry and its anisotropic material properties impose further restrictions for transmural or endocardial LV measurements. While lateral and posterior wall measurements are possible by placing the mouse in the right decubitus position, RV measurements may prove particularly challenging to accomplish. It is also imperative that circumferential measurements are also conducted. However, technically, it is currently impossible to collect concurrent longitudinal and circumferential measurements. Furthermore, although the investigation of the influencing effects of the myocardial sensor positions and their geometrical arrangements on strain (especially the relations of radial, longitudinal, circumferential, torsional, and principle strains) and force data are critically important for validation purposes, this is beyond the scope of this study but represents work-in-progress.

## 5. Conclusion

The presented approaches led to the successful implementation of procedures that allow *in vivo* force, displacement, and strain measurements. Future work will focus on accurate quantification of the underlying contributors (cardiomyocyte stiffening versus extracellular fibrosis) to altered global contractile status in transgenic and diseased myocardium.

## Acknowledgments

The authors are grateful to Prof H Rockman at Duke University Medical Center, USA for providing us with the wild-type and transgenic animals. Thanks are also attributed to Dr K Kleopas and Dr G Lapathitis at the Cyprus Institute of Neurology and Genetics for the permission to house the transgenic animals at the mouse facility before experimentations. We also thank Mr S Angeli at U. Cyprus for the development of tracking algorithms and for the motional analyses of myocardial studies and useful discussions. Dr G Kalogeros of

Sonometrics Inc. is also thanked for useful discussions and his support and help with the setup, calibration, and technical issues in regards to the use of piezoelectric crystals, and Dr J Bone (Kronex Inc.) for his support with the force sensors.

The senior author (CC) is also grateful to the ex-Directors of the Veterinary Services of the Ministry of Agriculture, Drs G Neophytou, C Kakoyiannis and P Toumazou, and to Veterinarians Drs I Ioannou, Y Ioannou, S Savva and T Pierides, for all their support towards the pursuit and completion of this study.

## Grants

This study was supported in part from the grant IPE/TECHNOLOGY/MHXAN/0609(BE)/05 from the Research Promotion Foundation in Cyprus.

## Disclosures

The authors have nothing to disclose. There are no conflicts of interest.

## Author Contributions

1. Conception and design of the experiments: CC, MM, SG
2. Collection, analysis, and interpretation of data: MM, CC, SG
3. Drafting the article or revising it critically for important intellectual content: CC, MM, SG

## References

- Alessi D R, Corrie J E, Fajer P G, Ferenczi M A, Thomas D D, Trayer I P and Trentham D R 1992 Synthesis and properties of a conformationally restricted spin-labeled analog of ATP and its interaction with myosin and skeletal muscle *Biochemistry* **31** 8043–54
- Aletras A, Ding S, Balaban R S and Wen H 1999 DENSE: displacement encoding with stimulated echoes in cardiac functional MRI *J. Magn. Reson.* **137** 247–52
- Arber S, Hunter J J, Ross J Jr, Hongo M, Sansig G, Borg J, Perriart J C, Chien K R and Caroni P 1997 MLP-Deficient mice exhibit a disruption of cardiac cytoarchitectural organization, dilated cardiomyopathy, and heart failure *Cell* **88** 393–403
- Axel L and Dougherty L 1989 MR Imaging of motion with spatial modulation of magnetization *Radiology* **171** 841–5
- Baker A J, Redfern C H, Harwood M D, Simpson P C and Conklin B R 2001 Abnormal contraction caused by expression of *G(i)*-coupled receptor in transgenic model of dilated cardiomyopathy *Am. J. Physiol. Heart Circ. Physiol.* **280** H1653–9 (PMID: 11247776)
- Brede M, Hadamek K, Meinel L, Wiesmann F, Peters J, Engelhardt S, Simm A, Haase A, Lohse M J and Hein L 2001 Vascular hypertrophy and increased P70S6 kinase in mice lacking the angiotensin II AT(2) receptor *Circulation* **104** 2602–7
- Choi H F, D'hooge J, Rademakers F E and Claus P 2010 Influence of left-ventricular shape on passive filling properties and end-diastolic fiber stress and strain *J. Biomech.* **43** 1745–53
- Choi H F, Rademakers F E and Claus P 2011 Left-ventricular shape determines intramyocardial mechanical heterogeneity *Am. J. Physiol.* **301** H2351–61
- Constantinides C, Mean R and Janssen B J 2011a Effects of isoflurane anesthesia on the cardiovascular function of the C57BL/6 mouse *ILAR J.* **52** 21–31
- Constantinides C, Angeli S and Mean R 2011b Murine cardiac hemodynamics following manganese administration under isoflurane anesthesia *Ann. Biomed. Eng.* **39** 2706–20 (PMID: 21677360)
- Demer L and Yin F C P 1983 Passive biaxial mechanical properties of isolated canine myocardium *J. Physiol.* **339** 615–30

- de Simone G, Devereux R B, Volpe M, Camargo M J, Wallerson D C and Laragh J H 1992 Relation of left ventricular hypertrophy, afterload, and contractility to left ventricular performance in Goldblatt hypertension *Am. J. Hypertension* **5** 292–301 (PMID: 1533770)
- Engel D, Peshock R, Armstrong R C, Sivasubramanian N and Mann D L 2004 Cardiac myocyte apoptosis provokes adverse cardiac remodeling in transgenic mice with targeted TNF overexpression *Am. J. Physiol. Heart Circ. Physiol.* **287** H1303–11
- Epstein F H 2007 MR in mouse models of cardiac disease *NMR Biomed.* **20** 238–55
- Esposito G, Santana L F, Dilly K, Cruz J D, Mao L, Lederer W J and Rockman H A 2000 Cellular and functional defects in a mouse model of heart failure *Am. J. Physiol. Heart Circ. Physiol.* **279** H3101–12 (PMID: 11087268)
- Esposito G, Rapacciuolo A, Naga Prasad S V, Takaoka H, Thomas S A, Koch W J and Rockman H A 2002 Genetic alterations that inhibit *in vivo* pressure-overload hypertrophy prevent cardiac dysfunction despite increased wall stress *Circulation* **105** 85–92
- Franco F, Dubois S K, Peshock R M and Shoheit R V 1998 Magnetic resonance imaging accurately estimates LV mass in a transgenic mouse model of cardiac hypertrophy *Am. J. Physiol.* **274** H679–83 (PMID: 9486274)
- Gilson W D, Yang Z, French B A and Epstein F H 2005 Measurement of myocardial mechanics in mice before and after infarction using multislice displacement-encoded MRI with 3D motion encoding *Am. J. Physiol.* **288** H1491–7
- Guan Q, Lu M, Wang X and Jiang C 2012 Solid dynamic models for analysis of stress and strain in human hearts *Comput. Math. Methods Med.* **2012** 634534
- Guccione J M, Costa K D and McCulloch A D 1995 Finite element stress analysis of left ventricular mechanics in the beating dog heart *J. Biomech.* **10** 1167–77
- Guccione J M, McCulloch A D and Waldman L K 1991 Passive material properties of intact ventricular myocardium determined from a cylindrical model *J. Biomech. Eng.* **113** 42–55
- Hanley J P and Loiselle D S 1998 Mechanisms of force inhibition by halothane and isoflurane in intact rat cardiac muscle *J. Physiol.* **506** 231–44
- He Z, Stienen G J, Barends J P and Ferenczi M A 1998 Rate of phosphate release after photoliberation of adenosine 5'-triphosphate in slow and fast skeletal muscle fibers *Biophys. J.* **75** 2389–401
- He Z H, Bottinelli R, Pellegrino M A, Ferenczi M A and Reggiani C 2000 ATP consumption and efficiency of human single muscle fibers with different myosin isoform composition *Biophys. J.* **79** 945–61
- Huisman R M, Elzinga G, Westerhof N and Sipkema P 1980 Measurement of left ventricular wall stress *Cardiovasc. Res.* **14** 142–53
- Kang T, Humphrey J D and Yin F C 1996 Comparison of biaxial mechanical properties of excised endocardium and epicardium *Am. J. Physiol. Heart Circ. Physiol.* **270** H2169–76 (PMID: 8764270)
- Knoll R *et al* 2010 A common MLP (Muscle LIM Protein) variant is associated with cardiomyopathy *Circ. Res.* **106** 695–704
- Krittian S, Janoske U, Oertel H and Bohlke T 2010 Partitioned fluid-solid coupling for cardiovascular blood flow *Ann. Biomed. Eng.* **38** 1426–41
- Kroon W, Delhaas T, Bovendeerd P and Arts T 2009 Computational analysis of the myocardial structure: adaptation of cardiac myofiber orientations through deformation *Med. Image Anal.* **13** 346–53
- Lima J A C, Jeremy R, Guier W, Bouton S, Zerhouni E A, McVeigh E M C, Buchalter M B, Weisfeldt M L, Shapiro E P and Weiss J L 1993 Accurate systolic wall thickening by nuclear magnetic resonance imaging with tissue tagging: correlation with sonomicrometers in normal and ischemic myocardium *J. Am. Coll. Cardiol.* **21** 1741–51
- McCulloch A D, Smaill B H and Hunter P J 1989 Regional left ventricular epicardial deformation in the passive dog heart *Circ. Res.* **64** 721–33
- Nakano K, Sugawara M, Ishihara K, Kanazawa S, Corin W J, Denslow S, Biederman R W and Carabello B A 1990 Myocardial stiffness derived from end-systolic wall stress and logarithm of reciprocal of wall thickness contractility index independent of ventricular size *Circulation* **82** 1352–61
- Nevo E and Lanir Y 1994 The effect of residual strain on the diastolic function of the left ventricle as predicted by a structural model *J. Biomech.* **27** 1433–46
- Omens J H, Farr D D, McCulloch A D and Waldman L K 1996 Comparison of two techniques for measuring two-dimensional strain in rat left ventricles *Am. J. Physiol.* **271** H1256–61
- Omens J H, MacKenna D A and McCulloch A D 1993 Measurement of strain and analysis of stress in resting rat left ventricular myocardium *J. Biomech.* **26** 665–76

- Osman N F, Kerwin W S, McVeigh E R and Prince J L 1999 Cardiac motion tracking using CINE harmonic phase (HARP) magnetic resonance imaging *Magn. Reson. Med.* **42** 1048–60
- Pelle G, Ohayon J, Oddou C and Brun P 1984 Theoretical models in mechanics of the left ventricle *Biorheology* **21** 709–22 (PMID: 6394067)
- Pinto J G and Fung Y C 1973 Mechanical properties of the heart muscle in the passive state *J. Biomech.* **6** 597–616
- Rockman H A, Ross R S, Harris A N, Knowlton K U, Steinhilber M E, Field L J, Ross J and Chien K R 1991 Segregation of atrial-specific and inducible expression of an atrial natriuretic factor transgene in an *in vivo* murine model of cardiac hypertrophy *Proc. Natl Acad. Sci. USA* **88** 8277–81
- Schmid H, O'Callaghan P, Nash M P, Lin W, LeGrice I J, Smaill B H, Young A A and Hunter P J 2008 Myocardial material parameter estimation *Biomech. Model Mechanobiol.* **7** 161–73
- Schmid P, Stuber M, Boesiger P, Hess O M and Niederer P 1995 Determination of displacement, stress- and strain-distribution in the human heart: a FE-model on the basis of MR imaging *Technol. Health Care* **3** 209–14 (PMID: 8749867)
- Takaoka H, Esposito G, Mao L, Suga H and Rockman H A 2002 Heart size-independent analysis of myocardial function in murine pressure overload hypertrophy *Am. J. Physiol. Heart Circ. Physiol.* **282** H2190–7
- Takayama Y, Costa K D and Covell J W 2002 Contribution of laminar myofiber architecture to load-dependent changes in mechanics of LV myocardium *Am. J. Physiol. Heart Circ. Physiol.* **282** H1510–20
- Unsold B *et al* 2012 Age-dependent changes in contractile function and passive elastic properties of myocardium from mice lacking muscle LIM protein (MLP) *Eur. J. Heart Failure* **14** 430–7
- Vetter F J and McCulloch A D 2000 Three-dimensional stress and strain in passive rabbit left ventricle: a model study *Ann. Biomed. Eng.* **28** 781–92
- Villarreal F J, Waldman L K and Lew W Y 1988 Technique for measuring regional two-dimensional finite strains in canine left ventricle *Circ. Res.* **62** 711–21
- Waldman L K, Fung Y C and Covell J W 1985 Transmural myocardial deformation in the canine left ventricle. Normal *in vivo* three-dimensional finite strains *Circ. Res.* **57** 152–63
- Weis S M, Emery J L, Becker D, McBride D J Jr, Omens J H and McCulloch A D 2000 Myocardial mechanics and collagen structure in the osteogenesis imperfecta murine (oim) *Circ. Res.* **87** 663–9
- Wilding J R, Schneider J E, Sang A E, Davies K E, Neubauer S and Clarke K 2005 Dystrophin- and MLP-deficient mouse hearts: marked differences in morphology and function, but similar accumulation of cytoskeletal proteins *FASEB J.* **19** 79–81
- Wu X, Haystead T A, Nakamoto R K, Somlyo A V and Somlyo A P 1998 Acceleration of myosin light chain dephosphorylation and relaxation of smooth muscle by telokin. Synergism with cyclic nucleotide-activated kinase *J. Biol. Chem.* **273** 11362–9
- Yamaguchi M and Takemori S 2001 Activating efficiency of Ca<sup>2+</sup> and cross-bridges as measured by phosphate analog release *Biophys. J.* **80** 371–8
- Yeon S B, Reichek N, Tallant B A, Lima J A, Calhoun L P, Clark N R, Hoffman E A, Ho K K and Axel L 2001 Validation of *in vivo* myocardial strain measurement by magnetic resonance tagging with sonomicrometry *J. Am. Coll. Cardiol.* **38** 555–61
- Yin F C P, Strumpf R K, Chew P H and Zeger S L 1987 Quantification of the mechanical properties of noncontracting canine myocardium under simultaneous biaxial loading *J. Biomech.* **20** 577–89
- Zerhouni E A, Parish D M, Rogers W J, Yang A and Shapiro E P 1988 Human heart: tagging with MR imaging—a method for noninvasive assessment of myocardial motion *Radiology* **169** 59–63
- Zhong X, Spottiswoode B S, Meyer C H, Kramer C M and Epstein F H 2010 Imaging three-dimensional myocardial mechanics using navigator-gated volumetric spiral cine DENSE MRI *Magn. Reson. Med.* **64** 1089–97
- Zhong X, Gibberman L B, Spottiswoode B S, Gilliam A D, Meyer C H, French B A and Epstein F H 2011 Comprehensive cardiovascular magnetic resonance of myocardial mechanics in mice using three-dimensional cine DENSE *J. Cardiovasc. Magn. Reson.* **13** 83